Extremely large magnetoresistance induced by Zeeman effect-driven electron-hole compensation and topological protection in $MoSi_2$

M. Matin,[1,2] Rajib Mondal,[1] N. Barman,[2] A. Thamizhavel,[1] and S. K. Dhar[1]
[1]*Department of Condensed Matter Physics and Materials Science, Tata Institute of Fundamental Research, Homi Bhabha Road, Colaba, Mumbai 400 005, India*
[2]*Department of Physics, Dinhata College, Dinhata 736 135, West Bengal, India*

(Received 29 December 2017; published 24 May 2018)

Here, we report an extremely large positive magnetoresistance (XMR) in a single-crystal sample of $MoSi_2$, approaching almost 10^7% at 2 K in a 14-T magnetic field without appreciable saturation. Hall resistivity data reveal an uncompensated nature of $MoSi_2$ with an electron-hole compensation level sufficient enough to expect strong saturation of magnetoresistance in the high-field regime. Magnetotransport and the complementary de Haas–van Alphen (dHvA) oscillations results, however, suggest that strong Zeeman effect causes a magnetic field-induced modulation of the Fermi pockets and drives the system towards perfect electron-hole compensation condition in the high-field regime. Thus, the nonsaturating XMR of this semimetal arises under the unconventional situation of Zeeman effect-driven electron-hole compensation, whereas its huge magnitude is decided solely by the ultralarge value of the carrier mobility. Intrinsic ultralarge carrier mobility, strong suppression of backward scattering of the charge carriers, and nontrivial Berry phase in dHvA oscillations attest to the topological character of $MoSi_2$. Therefore, this semimetal represents another material hosting combination of topological and conventional electronic phases.

DOI: 10.1103/PhysRevB.97.205130

I. INTRODUCTION

Extremely large positive magnetoresistance (XMR) of bismuth, a prototype elemental semimetal, has been known for a long time [1]. Recently, the interest in magnetoresistance has been renewed due to the observation of positive XMR in WTe_2, which does not show saturation even in magnetic fields as high as 60 T [2]. The XMR in WTe_2 was followed by similar observations in several other semimetals. For example, an XMR $\sim 4 \times 10^6$% at 2 K in a 14-T magnetic field has been reported in $PtBi_2$ [3]. The other semimetals with comparable XMR are NbP, LaSb, NbAs, TaP, TaAs, $MoTe_2$, and MoP_2 [4–10]. The topological protection is invoked to account for the XMR in all these semimetals except LaSb, which exhibits XMR in a perfect electron-hole compensation situation [3,5,11–16]. Thus, XMR constitutes a major distinctive feature of the topological semimetals, and is often used as primary criteria for identifying newer material belonging to this class. An experimental study in late 1986 reported $MoSi_2$ to have an XMR $\sim 10^6$% at 4.2 K in a 7.4-T magnetic field [17]. Despite having such huge MR, $MoSi_2$ has never been studied to check whether the topological notion can be extended to this semimetal. Moreover, the contradicting interpretations suggested by the previous studies make the explanation of XMR in $MoSi_2$ based on electron-hole compensation highly controversial [18,19], and thus the validation of the electron-hole compensation mechanism for this semimetal still remains an open problem.

Here, we present a detailed study of the magnetotransport properties on single-crystal samples of $MoSi_2$. We have also probed de Haas–van Alphen (dHvA) oscillations and performed electronic structure calculations to complement our study. A $MoSi_2$ sample exhibits nonsaturating XMR $\sim 10^7$% at 2 K in a 14-T field, which is larger than the XMR values reported in the best known XMR semimetals of recent time. In contrast to the previous consensus of perfect electron-hole compensation in $MoSi_2$, predicted to be originated from an exact balancing of the volume of the Fermi pockets [18], we rather find a largely uncompensated nature of this semimetal. However, Zeeman effect causes a field-induced modulation of the Fermi pockets in a nontrivial way and drives the system towards a perfect electron-hole compensation condition in the high-field regime; the unprecedented large nonsaturating magnetoresistance in $MoSi_2$ arises due to the combined effect of Zeeman effect-driven carrier compensation and ultralarge carrier mobility. Additionally, strong suppression of backward scattering of the charge carriers, nontrivial Berry phase in dHvA oscillations, and paramagnetic singularity of dc magnetic susceptibility near zero field provide compelling evidences for the existence of topological state in $MoSi_2$.

II. MATERIAL AND METHODS

A single-crystal of $MoSi_2$ was grown by Czochralski method in a tetra-arc furnace. The as-grown single-crystal has a tetragonal structure (space group, *I*4/*mmm*; number, 139) with lattice parameters $a = b = 3.2045$ Å and $c = 7.8414$ Å. The magnetotransport measurements were performed in a 14-T physical property measurement system from Quantum Design, Inc. with sense current *I* parallel to the crystallographic *a* axis and field applied along the *c* axis, and vice versa. The dHvA oscillations were probed through magnetization measurements in a 14-T vibrating sample magnetometer from Quantum Design. The electronic structure calculations were performed within the density functional theory framework, as

implemented in the QUANTUM ESPRESSO code [20]. The generalized gradient approximation of Perdew *et al.* [21] was used for the exchange-correlation potential. The electronic wave functions were expanded in terms of plane-wave basis sets, and the pseudopotential approach was adopted for the calculations.

III. RESULTS AND DISCUSSION

As shown in Fig. 1(a) the electrical resistivity ρ_{xx} of $MoSi_2$, measured in the absence of magnetic field and with current along the a axis, exhibits metallic behavior in the temperature range 2–300 K, with ρ_{xx} decreasing steeply as temperature is lowered from 100 to 15 K. The steep decrement in ρ_{xx} implies strong enhancement in the transport lifetime of the charge carriers, which results in an extremely small residual resistivity

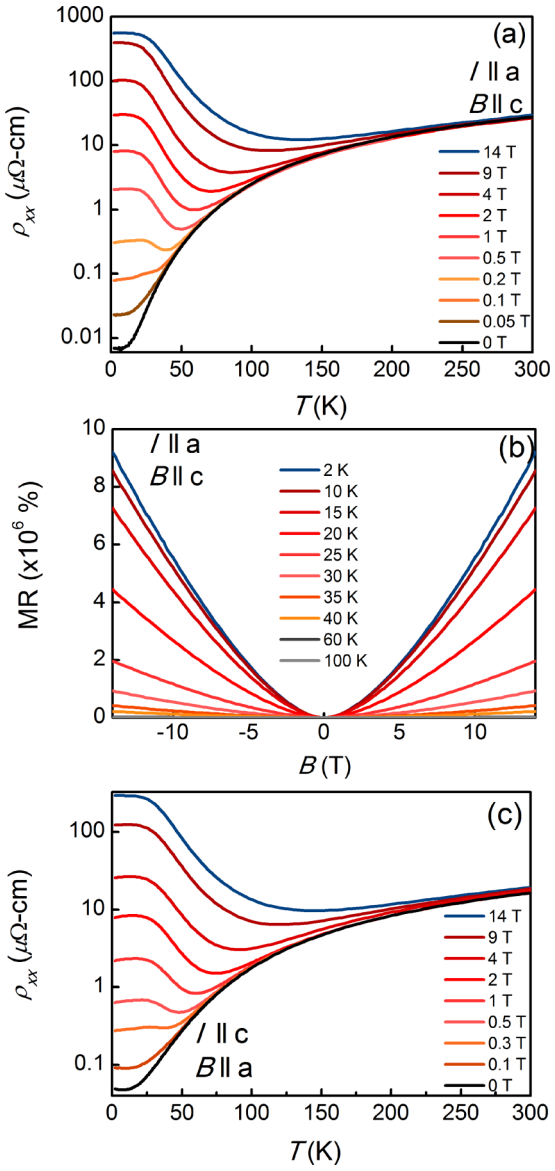

FIG. 1. Magnetotransport property of $MoSi_2$. (a) Temperature dependence of resistivity ρ_{xx} for $I \perp B \parallel c$ under a few representative transverse magnetic fields between zero and 14 T. (b) Corresponding transverse MR as a function of magnetic field at few selected temperatures between 2 and 100 K. (c) $\rho_{xx}(T)$ for $I \perp B \parallel a$ under different representative transverse magnetic fields up to 14 T.

$\rho_0 = 7.1$ nΩ cm and a large residual resistivity ratio (RRR) ~ 3926. The present RRR value is more than twice the best RRR value reported earlier for this semimetal [17], attesting to a better quality of our $MoSi_2$ single crystal. Application of the transverse magnetic field along the c axis leads to a remarkable enhancement in ρ_{xx}, particularly at low temperatures. The MR at 2 K reaches a value as large as $9.1 \times 10^6\%$ in a 14-T magnetic field. Comparable XMR is observed in topological semimetals such as WTe_2, $PtBi_2$, and MoP_2 under a strong magnetic field exceeding 30 T [2,3,10]. The present XMR value also exceeds the previously reported value in $MoSi_2$ by almost one order of magnitude [17]. The low-temperature and low-field response of resistivity is much more appealing, showing MR as large as $10^3\%$ at 2 K in a small magnetic field of 0.1 T, suggesting potential application of $MoSi_2$ as a magnetic sensor. At present, there is a high demand for such a magnetic sensor in the low-field and low-temperature regime [22]. As shown in Fig. 1(b) the field dependence of MR exhibits nonsaturating behavior within the field range of our measurements between zero and 14 T. The magnetotransport results shows strong anisotropic behavior, as indicated by a relatively higher value of $\rho_0 = 48.8$ nΩ cm, smaller RRR $\sim$ 336, and strongly suppressed XMR ($\sim 3.8 \times 10^5\%$ at $T = 2$ K and $B = 14$ T) for $I \perp B \parallel a$; refer to Fig. 1(c).

The field dependence of dc magnetization (M) displays robust signature of dHvA oscillations superimposed on a diamagnetic background. The dHvA oscillation signal was extracted by subtracting the nonoscillatory background from the experimental $M(B)$ data. As shown in Fig. 2(a) the dHvA oscillations at 2 K for $B \parallel c$ are traceable down to a remarkably low magnetic field $\sim$1.7 T. The dHvA oscillation amplitude, however, diminishes drastically at higher temperature, and becomes hardly detectable above 15 K. Figure 2(b) shows the expanded detail of the oscillation patterns in the high-field regime. The dHvA oscillations at 2 K exhibit strong Zeeman effect, which manifests itself as splitting of the oscillation peaks. At temperatures above 3 K, the split peaks, however, merge into a single peak, consistent with Zeeman effect, in which thermal broadening of the Landau levels smears out the Zeeman splitting. At 2 K, Zeeman splitting is discernible down to almost 4 T, which is much smaller than the threshold magnetic field value $B > 17$ T for peak splitting in topological semimetal Cd_3As_2 with the highest carrier mobility reported so far [23–25]. Figure 2(c) shows the frequency spectra obtained by performing the fast Fourier transform (FFT) of the dHvA oscillations, revealing two principal frequencies $F_\alpha = 725$ T and $F_\beta = 825$ T, which are in close agreement with the previous dHvA result [18]. Temperature dependence of the oscillation amplitude shown in Fig. 2(d) is fitted using the thermal damping factor of Lifshitz-Kosevich formula [26]: $R_T = X/\sinh(X)$, where $X = \lambda T m^*/B$, $\lambda = 2\pi^2 k_B m_e/e\hbar$, m^* is the cyclotron effective mass in the unit of free electron mass m_e, and other terms have their usual meanings. The fitting parameter provides determination of m^*. From the magnetic field-induced damping of the oscillation amplitude, $R_B = \exp(-\lambda T_D m^*/B)$, the Dingle temperature T_D at 2 K is estimated; and the corresponding fittings are shown in the inset of Fig. 2(d). From the obtained values of m^* and T_D the quantum mobility $\mu_Q = e/2\pi k_B T_D m^*$ is estimated to be 2.30×10^3 and 2.33×10^3 cm^2 V^{-1} s^{-1} for the α and β band, respectively.

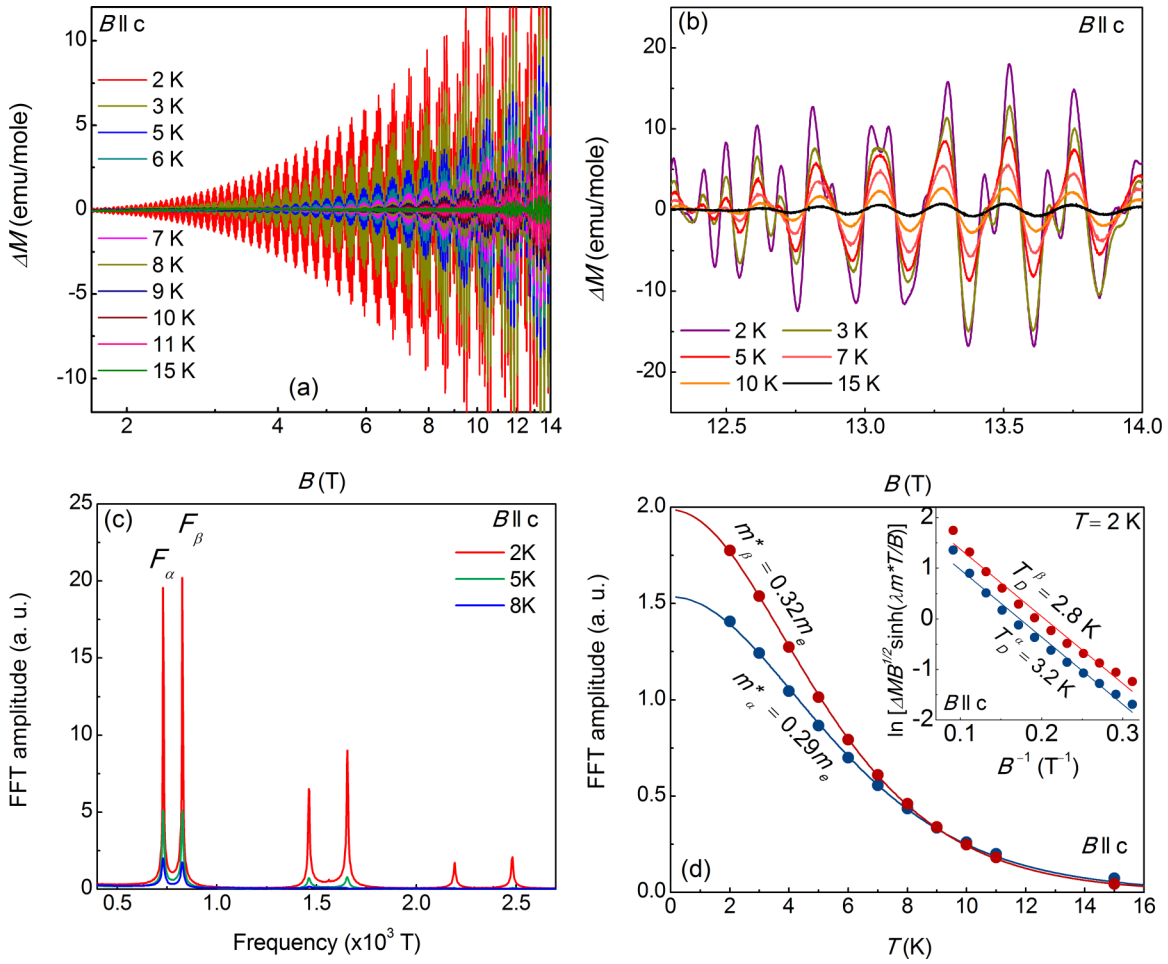

FIG. 2. dHvA oscillations in $MoSi_2$. (a, b) dHvA oscillations of magnetization for $B \parallel c$ at a few selected temperatures. The oscillation peaks at low temperature and high-field regime demonstrate Zeeman splitting. (c) Frequency spectrum corresponding to the dHvA oscillations, revealing two principle frequencies $F_\alpha = 725$ T and $F_\beta = 825$ T along with their second, third, and fourth harmonics. (d) Temperature dependence of the FFT amplitude at frequencies F_α and F_β (solid symbols). Solid lines are the fitted curves using the thermal damping factor of the Lifshitz-Kosevich formula. Inset: Dingle plots of the dHvA oscillations associated with the frequencies F_α and F_β.

The electronic band structure shown in Fig. 3(a) indicates the presence of two bands crossing the Fermi level, consistent with the dHvA oscillations result. The hole-type and the electron-type bands are centered at the high symmetric Γ and Z point, respectively. As shown in Fig. 3(b) the hole-type band has a cylindrical-shaped Fermi surface while the electron-type band has a Fermi surface with a shape of a four-cornered rosette.

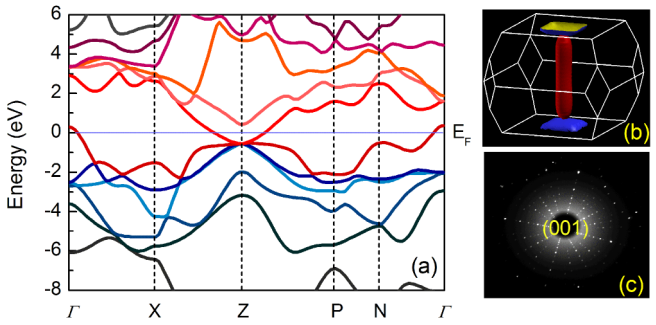

FIG. 3. (a) Electronic band structure of $MoSi_2$. (b) Fermi surfaces of $MoSi_2$ in the first Brillouin zone with a central hole pocket (cylindrical) and an electron pocket having the shape of a four-cornered rosette. (c) Laue diffraction pattern emphasizing the single-crystalline nature of the as-grown $MoSi_2$ single-crystal.

Having established plausible evidence for the presence of two bands participating in the charge transport mechanism in $MoSi_2$, we now use the classical theory of two-band transport for analyzing the magnetotransport data. According to the classical theory of two-band transport, the Hall resistivity ρ_{xy} and MR depend on magnetic field as [27,28]

$$\rho_{xy} = \frac{1}{e}\left[\frac{(p\mu_h^2 - n\mu_e^2)B + (p-n)\mu_e^2\mu_h^2B^3}{(p\mu_h + n\mu_e)^2 + (p-n)^2\mu_e^2\mu_h^2B^2}\right], \quad (1)$$

$$\mathrm{MR} = \frac{(n\mu_e + p\mu_h)^2 + (n\mu_e + p\mu_h)(p\mu_e + n\mu_h)\mu_e\mu_hB^2}{(n\mu_e + p\mu_h)^2 + (p-n)^2(\mu_e\mu_hB)^2} - 1 \quad (2)$$

where n (p) is the electron (hole) density and μ_e (μ_h) is the corresponding mobility. As shown in Fig. 4(a) the negative sign and sublinear behavior of $\rho_{xy}(B)$ at 2 K for $I \perp B \parallel a$ suggest an uncompensated nature of $MoSi_2$ with electrons

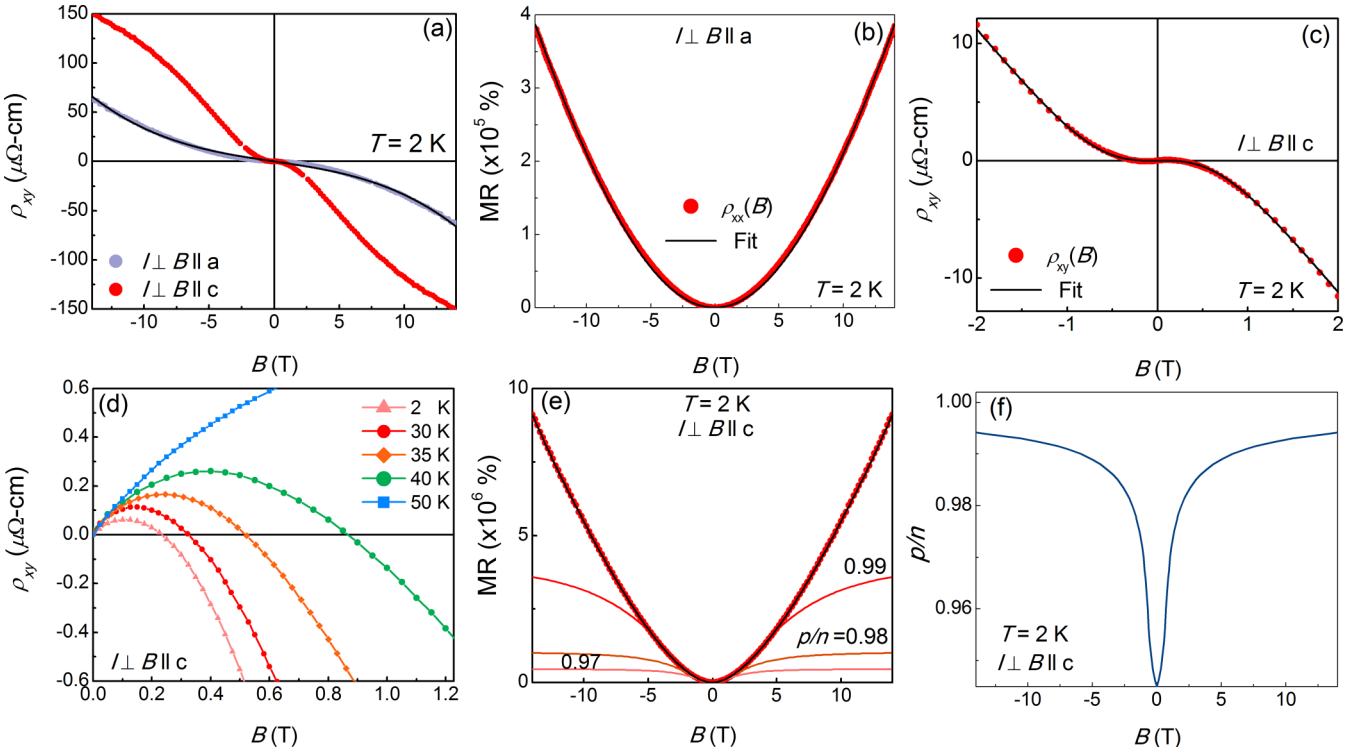

FIG. 4. Magnetotransport properties of $MoSi_2$ and the validation of the two-band model. (a) $\rho_{xy}(B)$ at 2 K for $I \perp B \parallel c$ and $I \perp B \parallel a$ (solid symbols). The black solid line represents the theoretical fit based on the two-band model Eq. (1). (b) Theoretical fitting of the MR data at 2 K for $I \perp B \parallel a$ based on Eq. (2). (c) Fitting of the $\rho_{xy}(B)$ data for $I \perp B \parallel c$ at 2 K and in the field regime below 2 T using Eq. (1). (d) $\rho_{xy}(B)$ for $I \perp B \parallel c$ at a few selected temperatures, demonstrating the sign reversal phenomenon in the low-field regime. (e) Field dependence of MR at 2 K for $I \perp B \parallel c$ (red solid symbols). The solid lines represents the MR calculated based on Eq. (2) using $\mu_e = 2.7 \times 10^5$ cm^2 V^{-1} s^{-1} and $\mu_h = 4.5 \times 10^5$ cm^2 V^{-1} s^{-1} and for three fixed values of $p/n = 0.97$, 0.98, and 0.99. (f) Magnetic field dependence of the compensation level p/n obtained from Eq. (2) using the values of $\mu_e = 2.7 \times 10^5$ cm^2 V^{-1} s^{-1} and $\mu_h = 4.5 \times 10^5$ cm^2 V^{-1} s^{-1}. In panel (e) the exact overlapping between the MR data and the simulated curve (black solid line) obtained from the $p/n(B)$ profile emphasizes the reliability of the estimation of p/n.

being the major carrier. The $\rho_{xy}(B)$ and the MR data at 2 K for $I \perp B \parallel a$ are simultaneously fitted to Eqs. (1) and (2). Satisfactory fits to the experimental data are achieved in the high-field regime, while in the low-field regime (1 to 5 T) the fitted curve slightly deviates from the experimental data. The fits shown in Figs. 4(a) and 4(b) give the compensation level $p/n = 0.989$, $\mu_e = 1.6 \times 10^5$ cm^2 V^{-1} s^{-1}, and $\mu_h = 9.8 \times 10^3$ cm^2 V^{-1} s^{-1}. However, if we perform the same exercise covering only the low-field regime up to 2 T, a value of $p/n = 0.947$ ($n = 7.93 \times 10^{20}$ cm^{-3}, $p = 7.51 \times 10^{20}$ cm^{-3}) and slightly different values of the carrier mobilities $\mu_e = 1.98 \times 10^5$ cm^2 V^{-1} s^{-1}, $\mu_h = 1.99 \times 10^4$ cm^2 V^{-1} s^{-1} are obtained. If the fit up to 2 T is extrapolated to higher fields, it deviates negatively from the $\rho_{xy}(B)$ data at high fields. This indicates an increase of the hole concentration with increasing field, which is in tune with the value of $p/n = 0.989$ as mentioned above.

The $\rho_{xy}(B)$ at 2 K for $I \perp B \parallel c$ is also negative, with similar implications as for $I \perp B \parallel a$. A noticeable feature of $\rho_{xy}(B)$ measured with $I \perp B \parallel c$ is its exhibition of positive curvature in the high-field regime; see Fig. 4(a). Equation (1) predicts a negative curvature of $\rho_{xy}(B)$ for a fixed value of p/n (<1), but a positive curvature may arise when the holes become increasingly important in the charge transport mechanism with increasing magnetic field. It is to be noted that the dHvA oscillation peaks for $B \parallel c$ exhibit strong Zeeman splitting, suggesting that the magnetic field-dependent behavior of the charge carriers is most likely due to the strong Zeeman effect. It is worth mentioning that Zeeman effect causes energy shifting of the Landau levels in the presence of magnetic field, and thereby reconstructs the Fermi pocket. In such case, the carrier density, being related to the size/shape of the Fermi pocket(s), also becomes magnetic field sensitive. Similar magnetic field-dependent behavior of p/n caused by Zeeman effect was also inferred for WTe_2 [29,30]. We have not yet carried out the dHvA measurement for $B \parallel a$ to check whether the data exhibit Zeeman effect, though our magnetotransport data discussed above suggest a similar behavior should occur. Figure S1 in the Supplemental Material shows the Shubnikov-de Haas (SdH) oscillations for $B \parallel a$ and $B \parallel c$ orientations [31]. While for $I \perp B \parallel c$ there is a distinct splitting of the SdH oscillation peaks similar to that observed in dHvA oscillations, for $I \perp B \parallel a$ there is a broadening of the SdH peaks which suggests that Zeeman effect is present even for this field orientation.

The two-band model equations fail to fit $\rho_{xy}(B)$ and MR data for $I \perp B \parallel c$ when the fitting field range is taken from zero to 14 T, which is apparently due to the magnetic field dependence of the model parameters n and p. Since $\rho_{xy}(B)$ (and also MR) depends less sensitively on the carrier density in the low-field regime, Eq. (1) successfully reproduces the $\rho_{xy}(B)$ data in the

low-field regime up to 2 T. The best fitting to $\rho_{xy}(B)$ data at 2 K, shown in Fig. 4(c), give $\mu_e = 2.7 \times 10^5$ cm^2 V^{-1} s^{-1}, $\mu_h = 4.5 \times 10^5$ cm^2 V^{-1} s^{-1}, $n = 1.75 \times 10^{21}$ cm^{-3}, $p = 1.67 \times 10^{21}$ cm^{-3}, and $p/n = 0.954$, which is comparable to the corresponding value for $I \perp B \parallel a$. It is notable that the minor-carrier holes have much higher mobility as compared to the major-carrier electrons. In several semimetals, lower population and higher mobility of the holes induce sign reversal of $\rho_{xy}(B)$ in the low-field regime [30,32,33]. Thus, the obtained values of the model parameters consistently explain the observation of sign reversal of $\rho_{xy}(B)$ for $I \perp B \parallel c$ shown in Fig. 4(d). The obtained values of the fitting parameters provide estimation of zero-field $\rho_{xx} = 1/e(n\mu_e + p\mu_h) = 5.1$ nΩ cm at 2 K, which is in close agreement with the experimental value of $\rho_0 = 7.1$ nΩ cm for $I \parallel a$. On the other hand, the zero-field ρ_{xx} at 2 K is estimated to be 36.3 nΩ cm for $I \parallel c$, consistent with the experimental value of $\rho_0 = 48.8$ nΩ cm for this current configuration. Evidently, the large difference between the zero-field $\rho_{xx}(T)$ for currents along the c and a axis, and hence the anisotropic magnetotransport behavior of $MoSi_2$, arises mainly because of the huge difference in carrier mobilities along these crystallographic directions.

However, a degree of compensation with $p/n = 0.954$ does not justify the magnitude of XMR as well as its nonsaturating behavior. Equation (2) predicts a strong saturation of MR even with $p/n = 0.97$; refer to Fig. 4(e). Such saturation effect is also observable even with $p/n = 0.99$, but to less extent. Thus, the nonsaturating behavior of XMR in $MoSi_2$ can only be understood if we consider the gradual improvement of compensation level towards a resonant situation with increasing magnetic field. The MR being an explicit function of p/n, μ_e, and μ_h (see Eqn. S1 and S2 in the Supplemental Material [34]), Eq. (2) provides estimation of p/n from the experimental MR data and the aforementioned values of μ_e and μ_h. The evolution of p/n with magnetic field is shown in Fig. 4(f) for $I \perp B \parallel c$. In zero field, $p/n = 0.946$, consistent with the value obtained from the analysis of $\rho_{xy}(B)$. As magnetic field is increased, p/n grows monotonically and becomes ~0.994 at 14 T, and such a variation of p/n consistently explains the nonsaturating behavior of $\rho_{xx}(B)$ as well as the positive curvature of $\rho_{xy}(B)$ observed in the high-field regime. Our analysis conclusively suggests that Zeeman effect-driven electron-hole compensation is crucial for boosting the nonsaturating XMR in $MoSi_2$. This unique behavior distinguishes $MoSi_2$ from other compensated semimetals belonging to this class. Interestingly, an uncompensated nature of this semimetal offers scope in driving the system towards a perfect compensation situation by increasing magnetic field. In that sense, $MoSi_2$ provides a platform where an imbalance between the charge carriers is found beneficial for realizing the XMR.

All the single-crystal samples of $MoSi_2$ studied so far including the present one exhibit extremely small ρ_0 in the range of 7–10 nΩ cm when current is along the a axis [17,35], indicating intrinsic ultralarge transport mobility of the charge carriers. The intrinsic ultralarge transport mobility and the accompanied XMR are characteristic of topological semimetals. Such intrinsic ultralarge transport mobility is originated from severe suppression of backward scattering of the charge carrier due to the topological protection. On the other hand, the quantum mobility μ_Q is sensitive to all

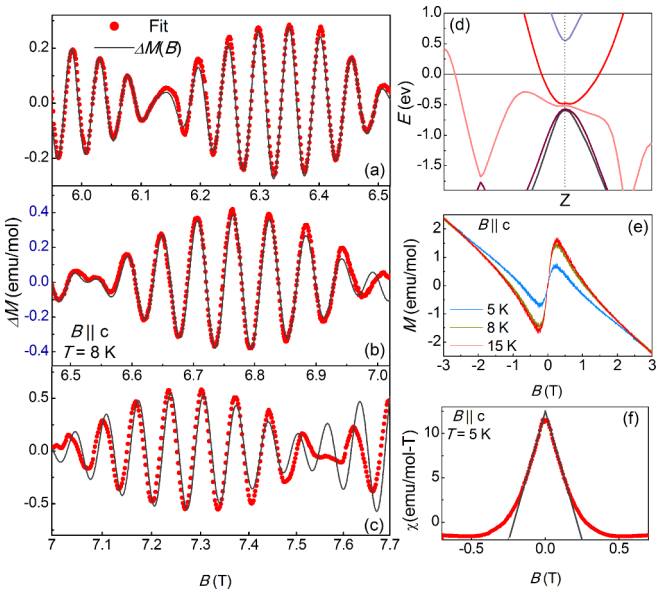

FIG. 5. (a–c) The dHvA oscillations at 8 K for $B \parallel c$. Solid symbols represent the experimental data and gray solid lines represent the theoretical fit based on Eq. (3). (d) Electronic band structure of $MoSi_2$ after including spin-orbit coupling. The figure is enlarged to show the absence of linear band inversion near the high symmetric Z point. (e) Magnetic field dependence of magnetization of $MoSi_2$ demonstrating the paramagnetic peak in the low-field regime. (f) Differential susceptibility $\chi = dM/dB$ as a function of magnetic field, exhibiting the paramagnetic singularity near zero field.

kinds of scattering mechanisms. Thus, the ratio $R_\mu = \mu_{tr}/\mu_Q$ quantifies the degree of suppression of the backward scattering. For $I \perp B \parallel c$, R_μ is estimated to be 193 for the holes, implying strong suppression of backward scattering.

Further experimental proof for the possible topological character of $MoSi_2$ may come from the Berry phase analysis. The Berry phase describes an additional geometrical phase factor acquired in the adiabatic evolution along a closed trajectory in the parameter space [36]. A nontrivial Berry phase manifests itself in observable effects in quantum oscillations. According to the Lifshitz-Kosevich formula for multiple frequencies, dHvA oscillation of magnetization is given by [26,37]

$$\Delta M = \sum_{i=\alpha,\beta} a_i B^{\frac{1}{2}} R_T^i R_B^i \sin[2\pi(F_i/B - \gamma_i)] \qquad (3)$$

where R_T and R_B describe the damping of oscillation amplitude due to temperature and magnetic field, respectively, and γ is related to the Berry phase factor f_B as $\gamma = 1/2 - f_B + \delta$. The parameter δ is an additional phase factor determined by the dimensionality, taking the values of zero and $\pm 1/8$ for two-dimensional (2D) and three-dimensional (3D) Fermi surfaces, respectively (plus and minus signs are, respectively, for holes and electrons) [38]. Starting from the previously estimated values of F, m^*, and T_D for α- and β-frequency branches, we perform a fully quantitative fitting of the dHvA oscillation pattern at 8 K using Eq. (3). For the fitting we restricted ourselves to only the high-temperature and low-field regime, where the experimental data are less likely affected by the Zeeman effect. As shown in Figs. 5(a)–5(c) the oscillation

pattern can be well reproduced by Eq. (3) with the values of F, m^*, and T_D that are close to their initial guess values, giving $\gamma_\alpha = -0.05$ and $\gamma_\beta = 0.23$. The α band represents an electron-type band as indicated by the negative sign of γ_α. The electron pocket shown in Fig. 3(b) has a quasi-2D nature, limiting the value of δ_α in the range of $-1/8 < \delta_\alpha < 0$ [38]. For the value of δ_α in this predicted range, the obtained γ_α can only be explained by considering $f_B = 1/2$. Such a value of f_B underlines the existence of topologically nontrivial electrons in $MoSi_2$. For the hole-type β band, γ_β deviates slightly from the 3D limiting value of $\gamma_\beta \equiv \delta_\beta = \pm 1/8$ expected for the topologically nontrivial holes, and corresponds to a Berry phase shift of 0.8π. This marginal deviation is likely due to the cylindrical shape of the hole pocket instead of a spherical one with perfect π Berry phase.

Despite several experimental evidences attesting the topological character of $MoSi_2$, the results of our *ab initio* calculations are not compatible with the picture of either Dirac or Weyl semimetal. The electronic structure does not exhibit any linear band inversion with distinct Dirac node/Weyl nodes after including the spin-orbit coupling; see Fig. 5(d). An alternative mechanism that may also account for the topological behavior of a material is the spin texture. Such spin texture may exist in the bulk state of a material with strong spin-orbit coupling, such as WTe_2 [39]. Owing to the d orbital of the heavy Mo atoms, strong spin-orbit coupling and the related spin texture are quite plausible in $MoSi_2$. The spin texture would exhibit observable effect in magnetic susceptibility χ. It was predicted theoretically that the resulting $\chi(B)$ shows a paramagnetic singularity near zero magnetic field with a linear field dependence [40]. Indeed, magnetization of $MoSi_2$ measured for $B \parallel c$ exhibits a clear paramagnetic contribution in the low-field regime; see Fig. 5(e). The corresponding differential susceptibility $\chi(= dM/dB)$ shown in Fig. 5(f) demonstrates paramagnetic singularity near zero field, varying linearly with magnetic field below 0.17 T. These observations suggest that, similar to WTe_2, the topological behavior of $MoSi_2$ is induced most likely due to the spin texture.

In conclusion, the electrons and holes in $MoSi_2$ are found to be largely uncompensated. Nevertheless, an extremely large nonsaturating transverse magnetoresistance $\sim 10^7\%$ at 2 K in a 14-T magnetic field is observed for $I \perp B \parallel c$. This unprecedented magnetoresistance without appreciable saturation in the high-field regime can be understood from the Zeeman effect-driven electron-hole compensation. Ultralarge mobility of both types of charge carriers reinforces the magnitude of the magnetoresistance. Strong suppression of backward scattering of the charge carriers and nontrivial Berry phase in dHvA oscillations attest to the topological character of $MoSi_2$. Spin texture possibly lends the topological character to this semimetal. In this regard, a spin-resolved photoemission experiment may be crucial in elucidating the origin of topological behavior of this exotic semimetal.

ACKNOWLEDGMENTS

We thank A. Maurya and D. Aoki for insightful conversations. We are also thankful to L. S. Sharath Chandra and S. B. Roy for critical reading of the paper.

[1] P. Kapitza, Proc. R. Soc. A **119**, 358 (1928).
[2] M. N. Ali, J. Xiong, S. Flynn, J. Tao, Q. D. Gibson, L. M. Schoop, T. Liang, N. Haldolaarachchige, M. Hirschberger, N. P. Ong, and R. J. Cava, Nature (London) **514**, 205 (2014).
[3] W. Gao, N. Hao, F.-W. Zheng, W. Ning, M. Wu, X. Zhu, G. Zheng, J. Zhang, J. Lu, H. Zhang, C. Xi, J. Yang, H. Du, P. Zhang, Y. Zhang, and M. Tian, Phys. Rev. Lett. **118**, 256601 (2017).
[4] C. Shekhar, A. K. Nayak, Y. Sun, M. Schmidt, M. Nicklas, I. Leermakers U. Zeitler, Y. Skourski, J. Wosnitza, Z. Liu, and Y. Chen, Nat. Phys. **11**, 645 (2015).
[5] F. F. Tafti, Q. D. Gibson, S. K. Kushwaha, N. Haldolaarachchige, and R. J. Cava, Nat. Phys. **12**, 272 (2016).
[6] N. J. Ghimire, Y. Luo, M. Neupane, D. J. Willams, E. D. Bauer, and F. Ronning, J. Phys.: Condens. Matter **27**, 152201 (2015).
[7] J. Hu, J. Y. Liu, D. Graf, S. M. A. Radmanesh, D. J. Adams, A. Chuang, Y. Wang, I. Chiorescu, J. Wei, L. Spinu, and Z. Q. Mao, Sci. Rep. **6**, 18674 (2016).
[8] C. Zhang, C. Guo, H. Lu, X. Zhang, Z. Yuan, Z. Lin, J. Wang, and S. Jia, Phys. Rev. B **92**, 041203(R) (2015).
[9] F. C. Chen, H. Y. Lv, X. Luo, W. J. Lu, Q. L. Pei, G. T. Lin, Y. Y. Han, X. B. Zhu, W. H. Song, and Y. P. Sun, Phys. Rev. B **94**, 235154 (2016).
[10] N. Kumar, Y. Sun, K. Manna, M. Yao, V. Süss, I. Leermakers, O. Young, T. Förster, M. Schmidt, H. Borrmann, B. Yan, U. Zeitler, M. Shi, and C. Felser, Nat. Commun. **8**, 1642 (2017).
[11] L. X. Yang, Z. K. Liu, Y. Sun, H. Peng, H. F. Yang, T. Zhang, B. Zhou, Y. Zhang, Y. F. Guo, M. Rahn, D. Prabhakaran, Z. Hussain, S.-K. Mo, C. Felser, B. Yan, and Y. L. Chen, Nat. Phys. **11**, 728 (2015).
[12] Y. Sun, S.-C. Wu, and B. Yan, Phys. Rev. B **92**, 115428 (2015).
[13] S.-Y. Xu, I. Belopolski, D. S. Sanchez, C. Zhang, G. Chang, C. Guo, G. Bian, Z. Yuan, H. Lu, T.-R. Chang, P. P. Shibayev, M. L. Prokopovych, N. Alidoust, H. Zheng, C.-C. Lee, S.-M. Huang, R. Sankar, F. Chou, C.-H. Hsu, H.-T. Jeng, A. Bansil, T. Neupert, V. N. Strocov, H. Lin, S. Jia, and M. Z. Hasan, Sci. Adv. **1**, e1501092 (2015).
[14] C. Wang, Y. Zhang, J. Huang, S. Nie, G. Liu, A. Liang, Y. Zhang, B. Shen, J. Liu, C. Hu, Y. Ding, D. Liu, Y. Hu, S. He, L. Zhao, L. Yu, J. Hu, J. Wei, Z. Mao, Y. Shi, X. Jia, F. Zhang, S. Zhang, F. Yang, Z. Wang, Q. Peng, H. Weng, X. Dai, Z. Fang, Z. Xu, C. Chen, and X. J. Zhou, Phys. Rev. B **94**, 241119(R) (2016).
[15] K. Deng, G. Wan, P. Deng, K. Zhang, S. Ding, E. Wang, M. Yan, H. Huang, H. Zhang, Z. Xu, J. Denlinger, A. Fedorov, H. Yang, W. Duan, H. Yao, S. Fan, H. Zhang, X. Chen, and S. Zhou, Nat. Phys. **12**, 1105 (2016).
[16] G. Autés, D. Gresch, M. Troyer, A. A. Soluyanov, and O. V. Yazyev, Phys. Rev. Lett. **117**, 066402 (2016).
[17] O. Laborde, O. Thomas, J. P. Senateur, and R. Madar, J. Phys. F **16**, 1745 (1986).

[18] J. M. van Ruitenbeek, W. Joss, R. Pauthenet, O. Thomas, J. P. Senateur, and R. Madar, Phys. Rev. B **35**, 7936 (1987).
[19] B. K. Bhattacharyya, D. M. Bylander, and L. Kleinman, Phys. Rev. B **32**, 7973 (1985).
[20] P. Giannozzi, S. Baroni, N. Bonini, M. Calandra, R. Car, C. Cavazzoni, D. Ceresoli, G. L. Chiarotti, M. Cococioni, I. Dabo, and A. D. Corso, J. Phys.: Condens. Matter **21**, 395502 (2009).
[21] J. P. Perdew, K. Burke, and M. Ernzerhof, Phys. Rev. Lett. **77**, 3865 (1996).
[22] J. Jankowski, S. El-Ahmar, and M. Oszwaldowski, Sensors **11**, 876 (2011).
[23] A. Narayanan, M. D. Watson, S. F. Blake, N. Bruyant, L. Drigo, Y. L. Chen, D. Prabhakaran, B. Yan, C. Felser, T. Kong, P. C. Canfield, and A. I. Coldea, Phys. Rev. Lett. **114**, 117201 (2015).
[24] J. Cao, S. Liang, C. Zhang, Y. Liu, J. Huang, Z. Jin, Z.-G. Chen, Z. Wang, Q. Wang, J. Zhao, and S. Li, Nat. Commun. **6**, 7779 (2015).
[25] Y. Zhao, H. Liu, C. Zhang, H. Wang, J. Wang, Z. Lin, Y. Xing, H. Lu, J. Liu, Y. Wang, S. M. Brombosz, Z. Xiao, S. Jia, X. C. Xie, and J. Wang, Phys. Rev. X **5**, 031037 (2015).
[26] D. Shoenberg, *Magnetic Oscillations in Metals* (Cambridge University, Cambridge, England, 2009).
[27] S. S. Murzin, S. I. Dorozhkin, G. Landwehr, and A. C. Gossard, J. Exp. Theor. Phys. Lett. **67**, 113 (1998).
[28] L. Wang, I. Gutiérrez-Lezama, C. Barreteau, N. Ubrig, E. Giannini, and A. F. Morpurgo, Nat. Commun. **6**, 8892 (2015).
[29] D. Rhodes, S. Das, Q. R. Zhang, B. Zeng, N. R. Pradhan, N. Kikugawa, E. Manousakis, and L. Balicas, Phys. Rev. B **92**, 125152 (2015).
[30] Y. Wang, K. Wang, J. Reutt-Robey, J. Paglione, and M. S. Fuhrer, Phys. Rev. B **93**, 121108(R) (2016).
[31] See Supplemental Material at http://link.aps.org/supplemental/10.1103/PhysRevB.97.205130 for Zeeman effect for both $B \parallel a$ and $B \parallel c$ field orientations and SdH oscillations for these field orientations.
[32] R. Singha, A. K. Pariari, B. Satpati, and P. Mandal, PNAS **114**, 2468 (2017).
[33] K. Wang, D. Graf, L. Li, L. Wang, and C. Petrovic, Sci. Rep. **4**, 7328 (2014).
[34] See Supplemental Material at http://link.aps.org/supplemental/10.1103/PhysRevB.97.205130 for the semiclassical two-band model equation, MR in terms of compensation level, and the carrier mobilities.
[35] F. Nava, E. Mazzega, M. Michelini, O. Laborde, O. Thomas, J. P. Senateur, and R. Madar, J. Appl. Phys. **65**, 1584 (1989).
[36] M. V. Berry, Proc. R. Soc. A **392**, 45 (1984).
[37] J. Hu, Z. Tang, J. Liu, X. Liu, Y. Zhu, D. Graf, K. Myhro, S. Tran, C. N. Lau, J. Wei, and Z. Mao, Phys. Rev. Lett. **117**, 016602 (2016).
[38] H. Murakawa, M. S. Bahramy, M. Tokunaga, Y. Kohama, C. Bell, Y. Kaneko, N. Nagaosa, H. Y. Hwang, and Y. Tokura, Science **342**, 1490 (2013).
[39] J. Jiang, F. Tang, X. C. Pan, H. M. Liu, X. H. Niu, Y. X. Wang, D. F. Xu, H. F. Yang, B. P. Xie, F. Q. Song and P. Dudin, T. K. Kim, M. Hoesch, P. K. Das, I. Vobornik, X. G. Wan, and D. L. Feng, Phys. Rev. Lett. **115**, 166601 (2015).
[40] L. Zhao, H. Deng, I. Korzhovska, Z. Chen, M. Konczykowski, A. Hruban, V. Oganesyan, and L. Krusin-Elbaum, Nat. Mat. **13**, 580 (2014).